JOURNAL OF MOLECULAR SPECTROSCOPY **190,** 130–139 (1998)
ARTICLE NO. MS987564

Sub-Millimeter-Wave Spectroscopy of the $Ar \cdot H_3^+$ and $Ar \cdot D_3^+$ Ionic Complexes

S. Bailleux,* M. Bogey,* H. Bolvin,* S. Civiš,*,[1] M. Cordonnier,* A. F. Krupnov,*,[2] M. Yu Tretyakov,*,[2] A. Walters,* and L. H. Coudert†

*Laboratoire de Spectroscopie Hertzienne, Centre d'Etudes et de Recherches Lasers et Applications, Université des Sciences et Technologies de Lille, F-59655 Villeneuve d'Ascq Cedex, France; †Laboratoire de Photophysique Moléculaire, C.N.R.S., Bâtiment 210, Université de Paris-Sud, F-91405 Orsay Cedex, France

Received January 13, 1998; in revised form February 23, 1998

An investigation of the sub-millimeter-wave spectra of the ionic complexes $Ar \cdot H_3^+$ and $Ar \cdot D_3^+$ is presented. These complexes were produced in a negative glow electric discharge, in mixtures of argon with either H_2 or D_2. About 80 new transitions were assigned in the 485–680 GHz frequency range using a sub-millimeter-wave spectrometer built with Russian made backward wave oscillators (BWO) sources. These measurements enabled us to observe the first $K_a = 2$ transitions for $Ar \cdot H_3^+$ and the first $K_a = 3$ transitions for $Ar \cdot D_3^+$. Analyses of the line frequencies were carried out using an IAM-like approach, which accounts for the large amplitude internal rotation motion displayed by both species. Insights into the geometry of the intermediate configuration for this large amplitude motion were gained.

1. INTRODUCTION

The weakly bound $Ar \cdot H_3^+$ ion and its isotopomers are the first ionic complexes for which high-resolution data could be recorded, about 10 years ago. It is only recently that two new ionic complexes have been detected in a supersonic-jet expansion: $Ar \cdot HCO^+$ by Fourier transform microwave spectroscopy (*1*) and $Ar \cdot HN_2^+$ by infrared spectroscopy using a tunable lead salt diode laser (*2*). However, the uniqueness of the unusual properties of the $Ar \cdot H_3^+$ ion and its isotopomers (for instance they display internal rotation about an axis perpendicular to the *a* axis) still makes their study an attractive field from the experimental as well as from the theoretical point of view. The first high-resolution spectra of the $Ar \cdot H_3^+$ and $Ar \cdot D_3^+$ ionic complexes were recorded in 1987 (*3*). Although a few lines were observed for both species, these measurements made it possible to obtain the structure of the ion and showed that it displays a large amplitude internal rotation motion leading to a splitting of the submillimeter lines. A detailed analysis of this tunneling motion was proposed in Ref. (*4*), where the measurements also were extended. Almost at the same time the first *ab initio* studies of $Ar \cdot H_3^+$ and of all its isotopic species (*5*) were published, and Escribano and Bunker (*6*) performed the first calculation of the tunneling splitting, with the help of a semirigid bender model Hamiltonian. Except for the measurement of one microwave line of $Ar \cdot D_3^+$, which was observed recently in a supersonic-jet expansion (*7*), there has been no recent high-resolution investigation of the spectra of $Ar \cdot H_3^+$ and its isotopomers.

In this paper, we present a reinvestigation of the sub-millimeter-wave spectra of $Ar \cdot H_3^+$ and $Ar \cdot D_3^+$. The measurements were carried out with a new setting of the spectrometer in Lille, which was described elsewhere (*8, 9*) and which included Russian-made components. Thanks to the extended operating range, it was possible to measure 30 new lines for $Ar \cdot H_3^+$ and 50 for its deuterated species and for both species the maximum K_a value in the data set was increased by one unit. The data were fitted by means of an internal-axis-method-like (IAM-like) formalism originally set up to treat the water dimer (*10, 11*) and which turns out to be a convenient tool to calculate tunneling splittings and their rotational dependence in nonrigid molecules (*12–14*). For both species, this formalism reproduces the observed frequency accurately and allows us to obtain information on the intermediate configuration for the large amplitude motion.

2. EXPERIMENT

The sub-millimeter-wave spectrometer used in this study already has been described extensively (*15*), but its operating range recently has been extended up to more than 900 GHz by Russian-constructed BWO tubes. The 2-m-long

[1] Permanent address: J. Heyrovský Institute of Physical Chemistry, Academy of Sciences of the Czech Republic, Dolejškova 3, 182 23 Prague 8, Czech Republic.

[2] Permanent address: Applied Physics Institute of Russian Academy of Sciences, 46 Uljanova Street, 603 600 Nizhnii Novgorod, Russia.

0022-2852/98 $25.00

absorption cell in Pyrex was equipped with a coil for generating a magnetic field, which allowed the extension of the negative glow DC discharge in which the ions, $Ar \cdot H_3^+$ and its fully substituted isotopomer $Ar \cdot D_3^+$, were generated. The plasma made from a mixture of argon and H_2 in the case of $Ar \cdot H_3^+$ (H_2 being replaced by D_2 for the production of $Ar \cdot D_3^+$) was cooled down by flowing liquid nitrogen in an outer jacket around the cell.

Some of the measurements reported in this work were performed using the experimental arrangement described previously (*16*) based on a Thomson BWO tube working from 415 to 470 GHz and on klystrons sources used with harmonic generation in the range 130–260 GHz. However, most of the measurements were carried out using a Russian-built BWO source (ISTOK) emitting in the range 483–680 GHz. With the help of a multiplier-mixer equipped with a planar Schottky diode (Institute for Applied Physics, Nizhnii Novgorod, Russia) as described in Ref. (*9*), the BWO source was phase-locked against a millimeter-wave frequency synthesizer (Kvarz, Russia) working in the 78–118 GHz region. Low noise detection was achieved by a liquid-helium cooled InSb detector (QMC Instruments, London). The millimeter-wave emission of the synthesizer was modulated at 40 kHz allowing frequency modulation of the power emitted from the BWO tube. The signal detected was demodulated at twice this frequency providing a second derivative lineshape. Frequency scanning, data acquisition, signal processing, and frequency measurement were controlled using an HP computer.

The best conditions for the generation of the ions were found to be P (Ar) = 10 mTorr, P (H_2 or D_2) = 10 mTorr (all pressures measured with the cell at room temperature) with a discharge voltage of 2 kV and a 21-mA steady current. The lines falling in the range of emission of the source and corresponding to $K_a = 0$ and 1 for $Ar \cdot H_3^+$, and $K_a = 0$, 1, and 2 for $Ar \cdot D_3^+$ were predicted from a least-squares analysis using previously measured transitions (*3, 4*) and were easily observed although shifted. We then looked for the previously unobserved $K_a = 2$ doublets of $Ar \cdot H_3^+$ and $K_a = 3$ quartets of $Ar \cdot D_3^+$. A first attempt at detecting the $Ar \cdot H_3^+$ doublets was unsuccessful, even after extending the width of the scan by up to 100 MHz around the predictions. On the other hand, we detected the $Ar \cdot D_3^+$ quartets close to the predictions, with an intensity ratio $I(K_a = 3)/I(K_a = 0)$ in good agreement with the theory. However, the K type and A–E splittings were not observed and the quartets were unresolved. We then decided to search very carefully for the missing $K_a = 2$ doublets of $Ar \cdot H_3^+$, both of symmetry E, corresponding to the $10_{2,9} \leftarrow 9_{2,8}$ and $10_{2,8} \leftarrow 9_{2,7}$ transitions. These lines lie in a range where the Russian source emits a maximum of power. We scanned with the same experimental conditions as described previously but with a higher time constant of the lock-in amplifier: 300 ms. We then found two

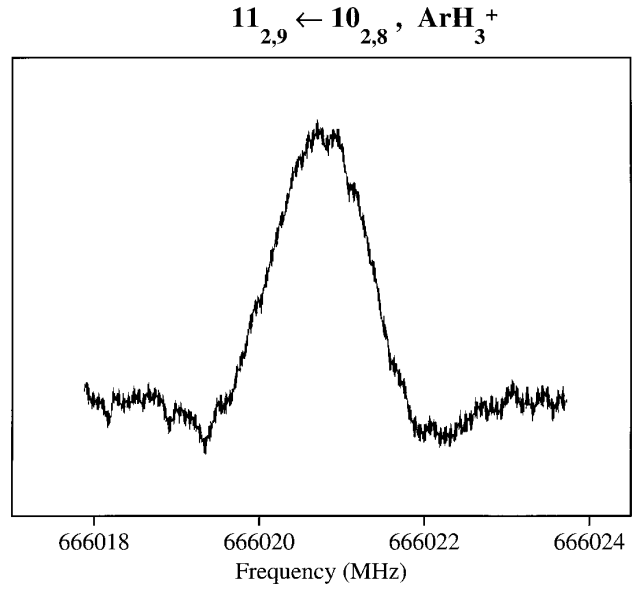

FIG. 1. Recording of the $K_a = 2$ transitions of $Ar \cdot H_3^+$:$11_{2,9} \leftarrow 10_{2,8}$ transition near 666 GHz.

extremely weak signals close to the predictions. Scanning for the next $K_a = 2$ components (corresponding to $J = 11$) led also to the detection of two signals as weak as the previous ones. It was then possible to identify all the $K_a = 2$ doublets lying in the range of emission of the source. The line intensities of these components were not as strong as expected. Finally, it was possible to measure 30 lines for $Ar \cdot H_3^+$ and 50 lines for $Ar \cdot D_3^+$ in the new frequency range. Figure 1 shows an example of a newly observed $K_a = 2$ transition of $Ar \cdot H_3^+$ (1000 points, 300 ms time constant). Figure 2 shows the newly detected $K_a = 3$ transition of $Ar \cdot D_3^+$. Examples of the stronger $K_a = 1$ for both isotopic species and of an A–E splitting transition of $Ar \cdot D_3^+$ also are given for illustration in Figs. 3, 4, and 5, respectively. All measured transitions, their observed frequency, and their observed minus calculated difference are listed in Table 1 for $Ar \cdot H_3^+$ and in Table 2 for $Ar \cdot D_3^+$.

3. THEORY

When calculating the tunneling-rotation energy of $Ar \cdot H_3^+$, the Coriolis coupling of the angular momentum generated by the large amplitude motion with the rotational angular momentum must be considered. As this interaction leads to a rotational dependence of the tunneling splitting, it must be taken into account when attempting to reproduce the microwave data of $Ar \cdot H_3^+$ as well as those of $Ar \cdot D_3^+$. In this section, the IAM-like formalism of Refs. (*10*) and (*11*), which provides a convenient method for computing this rotational dependence, is applied to such a calculation. When using this IAM-like approach, it is first

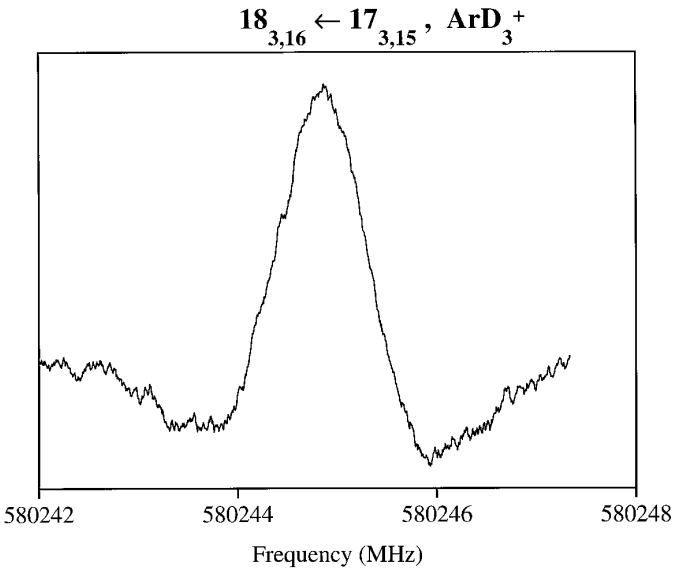

FIG. 2. Recording of the $K_a = 3$ transitions of $Ar \cdot D_3^+ : 18_{3,16} \leftarrow 17_{3,15}$ transition near 580 GHz.

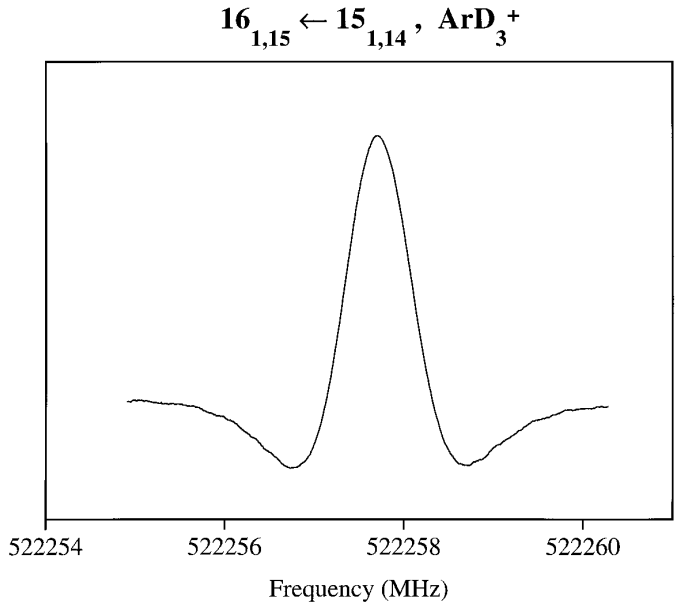

FIG. 4. Recording of the $16_{1,15} \leftarrow 15_{1,14}$ rotational transition of $Ar \cdot D_3^+$ near 522 GHz.

necessary to obtain the tunneling path(s) connecting the various nonsuperimposable configurations of the molecule in order to determine the contribution of each path to the J and K dependence of a Hamiltonian tunneling matrix element. In the case of $Ar \cdot H_3^+$, applying the IAM-like formalism is straightforward because there are only three nonsuperimposable equilibrium configurations and we will assume that there is only one tunneling path, corresponding to a 120° planar rotation of the H_3^+ group with respect to the argon atom. Using the IAM-like formalism still requires defining the set of coordinates needed to describe the various configurations of the molecule, choosing the symmetry group, generating symmetry-adapted wavefunctions, writing the Hamiltonian matrix, and deriving expressions for the tunneling matrix elements. These various steps will be car-

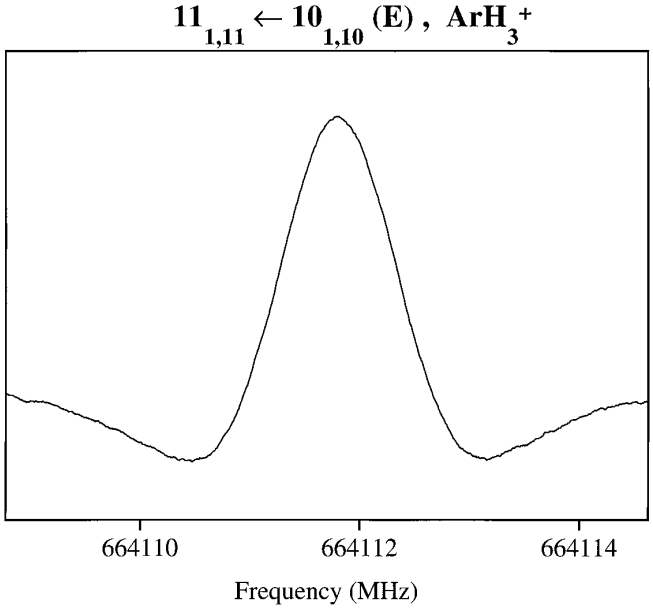

FIG. 3. Recording of the $11_{1,11} \leftarrow 10_{1,10}$ rotational transition of $Ar \cdot H_3^+$ near 664 GHz.

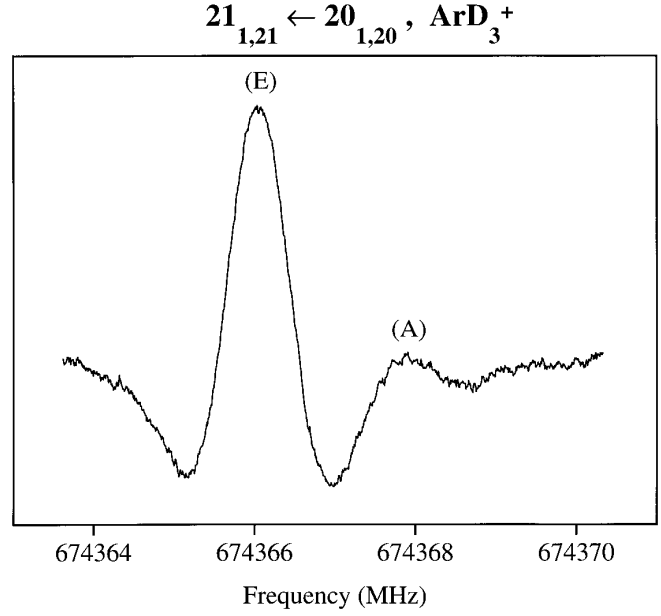

FIG. 5. Tunneling splitting of the $21_{1,21} \leftarrow 20_{1,20}$ transitions of $Ar \cdot D_3^+$ near 674 GHz.

TABLE 1
Measured Frequencies in the Spectrum[a] of $Ar \cdot H_3^+$

J'	K_a'	K_c'	Γ'	J''	K_a''	K_c''	Γ''	Obs.[b]	Diff.[c]	J'	K_a'	K_c'	Γ'	J''	K_a''	K_c''	Γ''	Obs.[b]	Diff.[c]
3	1	3	E''	2	1	2	E'	181846.579(150)	38	9	1	9	A_2''	8	1	8	A_2'	544219.620(150)	−85
3	1	3	A_2''	2	1	2	A_2'	181871.745(100)	123	9	2	8	E'	8	2	7	E''	545681.588(150)	−26
3	0	3	E''	2	0	2	E'	183234.594(100)	−3	9	2	7	E''	8	2	6	E'	545711.035(150)	3
3	1	2	E'	2	1	1	E''	184198.883(100)	−146	9	0	9	E''	8	0	8	E'	548257.711(150)	−43
3	1	2	A_2'	2	1	1	A_2''	184201.462(100)	−53	9	1	8	E'	8	1	7	E''	551144.053(150)	21
6	1	6	E'	5	1	5	E''	363345.902(40)	−4	9	1	8	A_2'	8	1	7	A_2''	551151.841(150)	31
6	1	6	A_2'	5	1	5	A_2''	363395.763(40)	−11	10	1	10	E'	9	1	9	E''	604194.208(150)	−245
6	0	6	E'	5	0	5	E''	366108.959(40)	−12	10	1	10	A_2'	9	1	9	A_2''	604276.308(150)	−48
6	1	5	E''	5	1	4	E'	368036.116(40)	6	10	2	9	E''	9	2	8	E'	605891.759(150)	−11
6	1	5	A_2''	5	1	4	A_2'	368041.152(40)	−10	10	2	8	E'	9	2	7	E''	605932.090(150)	−7
7	1	7	E''	6	1	6	E'	423707.936(100)	54	10	0	10	E'	9	0	9	E''	608748.208(150)	−31
7	1	7	A_2''	6	1	6	A_2'	423765.918(100)	25	10	1	9	E''	9	1	8	E'	611953.095(150)	8
7	0	7	E''	6	0	6	E'	426924.223(100)	80	10	1	9	A_2''	9	1	8	A_2'	611961.833(150)	12
7	1	6	E'	6	1	5	E''	429171.519(100)	31	11	1	11	E''	10	1	10	E'	664111.677(150)	154
7	1	6	A_2'	6	1	5	A_2''	429177.481(100)	53	11	1	11	A_2''	10	1	10	A_2'	664201.247(150)	82
8	1	8	E'	7	1	7	E''	483978.901(150)	−41	11	2	10	E'	10	2	9	E''	665967.288(150)	−10
8	1	8	A_2'	7	1	7	A_2''	484044.944(150)	−71	11	2	9	E''	10	2	8	E'	666020.866(150)	−22
8	1	7	E''	7	1	6	E'	490212.141(150)	23	11	0	11	E''	10	0	10	E'	669102.246(150)	5
8	1	7	A_2''	7	1	6	A_2'	490218.997(150)	31	11	1	10	E'	10	1	9	E''	672624.871(150)	−76
9	1	9	E''	8	1	8	E'	544145.652(150)	−11	11	1	10	A_2'	10	1	9	A_2''	672634.606(150)	−59

[a] In addition to the usual rotational quantum numbers, transitions are assigned with the symmetry species Γ' and Γ'' in D_{3h} of the upper and lower levels, respectively.
[b] Observed frequencies in MHz. Number in parentheses are uncertainties in the same units as the last digits.
[c] Observed minus calculated frequencies in kHz corresponding to the constants in Table 5.

ried out below. It should be pointed out that the present approach closely parallels that performed in Ref. (*14*) on the similar molecular system $C_2H_3^+$.

A. Coordinate System and Symmetry Considerations

In agreement with Escribano and Bunker (*6*), we take for the large amplitude coordinate the angle ρ defined in Fig. 1 of their paper. The equation relating the laboratory-fixed Cartesian coordinates to a set of molecule-fixed reference coordinates is the following:

$$\mathbf{R}_i = \mathbf{R} + S^{-1}(\chi, \theta, \phi)[\mathbf{a}_i(\rho) + \mathbf{d}_i], \quad i = 0\text{–}3, \quad [1]$$

where $\mathbf{R}_i$ and $\mathbf{R}$ are the position vectors in the laboratory of atom i and of the molecular center of mass, respectively; $S^{-1}(\chi, \theta, \phi)$ represents the usual 3×3 matrix, which transforms from the molecule-fixed coordinates to the laboratory-fixed coordinates, and which is characterized by the three Eulerian angles χ, θ, and ϕ; $\mathbf{a}_i(\rho)$ are reference positions for the atoms, which depend explicitly on the large amplitude coordinate ρ; and $\mathbf{d}_i$ are infinitesimal vibrational displacement vectors, which will be ignored in the remainder of this paper. The atoms are numbered so that 0 identifies the argon atom, and 1, 2, and 3 identify the three hydrogen atoms H_1, H_2, and H_3, in the same way as in Fig. 1 of Escribano and Bunker's paper (*6*). The reference positions $\mathbf{a}_i(\rho)$ also can be defined with the help of this figure. They are such that the molecular center of mass is at the origin of the molecule-fixed axis system. The H_3^+ triangle is contained in the *xz* plane; its center of mass and the argon atom are 2.385 Å apart, according to the results of Ref. (*6*), and they are both held fixed in the *xyz*-axis system and located on the *z* axis. This choice implies, because of the masses of the atoms involved, that the *x*, *y*, and *z* axes are respectively parallel to the *b*, *c*, and *a* axes; the I^r representation being used.

The calculations of Simandiras *et al.* (*5*) showed that the equilibrium structure of $Ar \cdot H_3^+$ has the argon atom close to a vertex of the H_3^+ triangle. As can be gathered from Eq. [1], the three nonsuperimposable equilibrium configurations, which will be numbered 1, 2, and 3, can therefore be characterized by equilibrium values of ρ equal, respectively, to 0, $2\pi/3$, and $4\pi/3$. This allows us to define the vibrational function corresponding to configuration *n* as

TABLE 2
Measured Frequencies in the Spectrum[a] of Ar · D_3^+

J'	K'_a	K'_c	Γ'	J''	K''_a	K''_c	Γ''	Obs.[b]	Diff.[c]	J'	K'_a	K'_c	Γ'	J''	K''_a	K''_c	Γ''	Obs.[b]	Diff.[c]
1	0	1	A_1''	0	0	0	A_1'	32616.241(100)*d*	−9	12	0	12	A_1'	11	0	11	A_1''	390272.418(40)	19
1	0	1	E''	0	0	0	E'	32616.241(100)	−9	12	1	11	E''	11	1	10	E'	392569.456(40)	79
4	1	4	E'	3	1	3	E''	129516.041(60)	146	13	0	13	E''	12	0	12	E'	422580.373(40)	3
4	0	4	A_1'	3	0	3	A_1''	130425.895(60)*d*	−13	13	0	13	A_1''	12	0	12	A_1'	422581.216(40)	28
4	0	4	E'	3	0	3	E''	130425.895(60)	−13	14	0	14	E'	13	0	13	E''	454837.299(40)	−18
4	1	3	E''	3	1	2	E'	131187.204(60)	−91	14	0	14	A_1'	13	0	13	A_1''	454838.207(40)	10
6	1	6	E'	5	1	5	E''	194199.844(60)	42	15	1	14	E'	14	1	13	E''	489920.609(40)*d*	96
6	0	6	A_1'	5	0	5	A_1''	195560.542(60)*d*	−41	15	1	14	A_2'	14	1	13	A_2''	489920.609(40)	96
6	0	6	E'	5	0	5	E''	195560.542(60)	−41	16	1	16	E'	15	1	15	E''	515674.189(40)	−61
6	1	5	E''	5	1	4	E'	196703.637(60)	−86	16	1	16	A_2'	15	1	15	A_2''	515675.617(40)	59
8	1	8	E'	7	1	7	E''	258794.644(60)	40	16	3	14	E'	15	3	13	E''	516465.421(100)*q*	−308
8	0	8	E'	7	0	7	E''	260600.837(60)	9	16	3	14	A_2'	15	3	13	A_2''	516465.421(100)	−308
8	0	8	A_1'	7	0	7	A_1''	260601.400(60)	67	16	3	13	E''	15	3	12	E'	516465.421(100)	−308
8	1	7	E''	7	1	6	E'	262127.188(60)	−34	16	3	13	A_2''	15	3	12	A_2'	516465.421(100)	−308
11	1	11	E''	10	1	10	E'	355453.705(40)	−34	16	2	15	E''	15	2	14	E'	518054.167(40)*d*	26
11	2	10	A_1'	10	2	9	A_1''	357105.962(40)*d*	−47	16	2	15	A_1''	15	2	14	A_1'	518054.167(40)	26
11	2	10	E'	10	2	9	E''	357105.962(40)	−47	16	2	14	E'	15	2	13	E''	518162.605(40)*d*	128
11	2	9	A_1''	10	2	8	A_1'	357141.252(40)*d*	−189	16	2	14	A_1'	15	2	13	A_1''	518162.605(40)	128
11	2	9	E''	10	2	8	E'	357141.252(40)	−189	16	0	16	E'	15	0	15	E''	519179.229(40)	1
11	0	11	E''	10	0	10	E'	357915.207(50)	−49	16	0	16	A_1'	15	0	15	A_1''	519180.244(40)	11
11	0	11	A_1''	10	0	10	A_1'	357915.935(50)	−14	16	1	15	E''	15	1	14	E'	522257.575(40)*d*	122
11	1	10	E'	10	1	9	E''	360019.410(40)	12	16	1	15	A_2''	15	1	14	A_2'	522257.575(40)	122
12	1	12	E'	11	1	11	E''	387595.942(40)	−85	17	1	17	E''	16	1	16	E'	547551.148(40)	−50
12	2	11	A_1''	11	2	10	A_1'	389395.436(40)*d*	−100	17	1	17	A_2''	16	1	16	A_2'	547552.694(40)	109
12	2	11	E''	11	2	10	E'	389395.436(40)	−100	17	3	15	E''	16	3	14	E'	548388.052(100)*q*	−146
12	2	10	A_1'	11	2	9	A_1''	389441.402(40)*d*	−112	17	3	15	A_2''	16	3	14	A_2'	548388.052(100)	−146
12	2	10	E'	11	2	9	E''	389441.402(40)	−112	17	3	14	E'	16	3	13	E''	548388.052(100)	−146
12	0	12	E'	11	0	11	E''	390271.630(40)	−14	17	3	14	A_2'	16	3	13	A_2''	548388.052(100)	−146

[a] In addition to the usual rotational quantum numbers, transitions are assigned with the symmetry species Γ' and Γ'' in $D_{3h}(M)$ of the upper and lower levels, respectively.
[b] Observed frequencies in MHz. Numbers in parentheses are uncertainties in the same units as the last digits. The letter *d* (*q*) indicates that the following line (the three following lines) were treated as unresolved doublets (quartets). The first line of this table is from Ref. [7].
[c] Observed minus calculated frequencies in kHz corresponding to the constants in Table 5.

$$\psi_n(\rho) = \exp - a\left\{1 - \cos\left[\rho - (n-1)\frac{2\pi}{3}\right]\right\}, \quad [2]$$

$n = 1$, 2, or 3.

In agreement with Escribano and Bunker (*6*), we adopt the $D_{3h}(M)$ molecular symmetry group for the present problem. A character table for this group can be found in Table A-9 of Ref. (*17*) and the effects of the various permutation-inversion symmetry operations on the Eulerian angles and on the large amplitude coordinate ρ of Eq. [1] are given in Table 3 of the present paper. With the help of these tables it can be shown that the vibrational functions of Eq. [2] can be generated applying an appropriate generating operation on the vibrational function of framework 1

$$\psi_2(\rho) = (132)\psi_1(\rho) \quad \text{and} \quad \psi_3(\rho) = (132)^2\psi_1(\rho). \quad [3]$$

These equations, along with Eq. [2], allow us to build the three symmetry-adapted linear combinations of vibrational functions $\psi_\Gamma(\rho)$, $\Gamma = A_1'$ or E', which are the following:

$$\psi_{A_1'}(\rho) = [\psi_1(\rho) + \psi_2(\rho) + \psi_3(\rho)]/\sqrt{3},$$
$$\psi_{E_a'}(\rho) = [2\psi_1(\rho) - \psi_2(\rho) - \psi_3(\rho)]/\sqrt{6}, \quad [4]$$
$$\psi_{E_b'}(\rho) = [\psi_2(\rho) - \psi_3(\rho)]/\sqrt{2}.$$

In these equations, the two component functions corresponding to the doubly degenerate symmetry species are distinguished by the subscripts *a* and *b* and are such that $(23)|E_a'\rangle = +|E_a'\rangle$ and $(23)|E_b'\rangle = -|E_b'\rangle$. These transformation properties will be taken as standard transformation properties throughout this paper for E'-symmetry as well as for E''-symmetry functions.

Symmetry-adapted rotational functions turn out also to be more convenient to write the Hamiltonian tunneling matrix elements of the next subsections. These symmetry-adapted

TABLE 2—*Continued*

J'	K'_a	K'_c	Γ'	J''	K''_a	K''_c	Γ''	Obs.[b]	Diff.[c]	J'	K'_a	K'_c	Γ'	J''	K''_a	K''_c	Γ''	Obs.[b]	Diff.[c]
17	2	16	E'	16	2	15	E''	550073.467(40)	−29	19	2	18	A'_1	18	2	17	A''_1	613909.747(40)	81
17	2	16	A'_1	16	2	15	A''_1	550073.924(40)	63	19	2	17	E''	18	2	16	E'	614089.912(40)*d*	192
17	2	15	E''	16	2	14	E'	550203.507(40)*d*	177	19	2	17	A''_1	18	2	16	A'_1	614089.912(40)	192
17	2	15	A''_1	16	2	14	A'_1	550203.507(40)	177	19	0	19	E''	18	0	18	E'	615198.734(40)	56
17	0	17	E''	16	0	16	E'	551255.793(40)	20	19	0	19	A''_1	18	0	18	A'_1	615199.894(40)	26
17	0	17	A''_1	16	0	16	A'_1	551256.516(40)	−323	19	1	18	E'	18	1	17	E''	618869.330(40)*d*	201
18	1	18	E'	17	1	17	E''	579362.991(40)	−14	19	1	18	A'_2	18	1	17	A''_2	618869.330(40)	201
18	1	18	A'_2	17	1	17	A''_2	579364.552(40)	80	20	1	20	E'	19	1	19	E''	642774.644(40)	17
18	3	16	E'	17	3	15	E''	580244.702(100)*q*	−49	20	1	20	A'_2	19	1	19	A''_2	642776.221(40)	−31
18	3	16	A'_2	17	3	15	A''_2	580244.702(100)	−49	20	3	18	E'	19	3	17	E''	643743.392(100)*q*	111
18	3	15	E''	17	3	14	E'	580244.702(100)	−49	20	3	18	A'_2	19	3	17	A''_2	643743.392(100)	111
18	3	15	A''_2	17	3	14	A'_2	580244.702(100)	−49	20	3	17	E''	19	3	16	E'	643743.392(100)	111
18	2	17	E''	17	2	16	E'	582026.743(40)	21	20	3	17	A''_2	19	3	16	A'_2	643743.392(100)	111
18	2	17	A''_1	17	2	16	A'_1	582027.191(40)	68	20	2	19	E''	19	2	18	E'	645717.400(40)	−8
18	2	16	E'	17	2	15	E''	582180.636(40)*d*	196	20	2	19	A''_1	19	2	18	A'_1	645717.873(40)	−18
18	2	16	A'_1	17	2	15	A''_1	582180.636(40)	196	20	2	18	E'	19	2	17	E''	645927.128(40)*d*	102
18	0	18	E'	17	0	17	E''	583263.742(40)	47	20	2	18	A'_1	19	2	17	A''_1	645927.128(40)	102
18	0	18	A'_1	17	0	17	A''_1	583264.862(40)	38	20	0	20	E'	19	0	19	E''	647056.373(40)	18
18	1	17	E''	17	1	16	E'	586736.247(40)*d*	204	20	0	20	A'_1	19	0	19	A''_1	647057.584(40)	−22
18	1	17	A''_2	17	1	16	A'_2	586736.247(40)	204	20	1	19	E''	19	1	18	E'	650925.763(40)*d*	151
19	1	19	E''	18	1	18	E'	611105.541(40)	−1	20	1	19	A''_2	19	1	18	A'_2	650925.763(40)	151
19	1	19	A''_2	18	1	18	A'_2	611107.092(40)	4	21	1	21	E''	20	1	20	E'	674366.021(40)	−3
19	3	17	E''	18	3	16	E'	612031.290(100)*q*	96	21	1	21	A''_2	20	1	20	A'_2	674367.705(40)	−23
19	3	17	A''_2	18	3	16	A'_2	612031.290(100)	96	21	3	19	E''	20	3	18	E'	675376.754(100)*q*	47
19	3	16	E'	18	3	15	E''	612031.290(100)	96	21	3	19	A''_2	20	3	18	A'_2	675376.754(100)	47
19	3	16	A'_2	18	3	15	A''_2	612031.290(100)	96	21	3	18	E'	20	3	17	E''	675376.754(100)	47
19	2	18	E'	18	2	17	E''	613909.747(40)*d*	81	21	3	18	A'_2	20	3	17	A''_2	675376.754(100)	47

rotational functions are Wang combinations of two symmetric top functions

$$|JK\alpha\rangle = 2^{-1/2}[|J, K\rangle + \alpha|J, -K\rangle], \qquad [5]$$

where $K \geq 0$, α equal $+1$ or -1, and $|J, K\rangle$ is the usual symmetric top function (without the dependence on the quantum number M, which is ignored for simplicity). For the special case $K = 0$, α must be set to $+1$ and the factor $2^{-1/2}$ becomes 2^{-1}. In Table 4 the symmetry species of these functions are given and depend on the parity of J and on their asymmetric-top labels.

Combining the vibrational functions of Eq. [2] and the rotational functions of Eq. [5], we can build the reference framework wavefunctions $\Psi_{JK\alpha n}$, $n = 1$, 2, or 3, which in the spirit of Ref. (*10*) are needed to solve the rovibrational-tunneling problem

$$\Psi_{JK\alpha n} = \psi_n(\rho) \cdot |JK\alpha\rangle, \quad n = 1, 2, \text{ or } 3. \qquad [6]$$

As it is wise to block-diagonalize the Hamiltonian matrix, we define, in a similar way, symmetry-adapted linear combinations of the above wavefunctions using the symmetry-adapted vibrational functions of Eqs. [4] and the rotational functions of Eq. [5]. These symmetry-adapted reference framework wavefunctions will be denoted $\Psi_{JK\alpha\Gamma}$, where Γ is their symmetry species, and they are the following:

$$\Psi_{JK\alpha\Gamma} = \psi_{\Gamma'}(\rho) \cdot |JK\alpha\rangle. \qquad [7]$$

In this equation, Γ' is the symmetry species of the vibrational function. Remembering that the latter symmetry species is either A'_1 or E', and that the rotational symmetry species is either A'_1, A'_2, A''_1, or A''_2, Eq. [7] implies that Γ can be any symmetry species of the $D_{3h}(M)$ molecular symmetry group. When Γ is a nondegenerate symmetry species, the rotational quantum numbers must be such that the rotational symmetry species is Γ. When Γ is a doubly degenerate symmetry species, the rotational symmetry species can be A'_1 or A'_2 for $\Gamma = E'$, and A''_1 or A''_2 for $\Gamma = E''$. The two component functions constructed with the help of Eq. [7] will obey the standard transformation properties defined in this subsection provided that Γ and Γ' correspond to the same (a or b) components for an A'_1 and an A''_1 rotational symmetry species, and to different components for an A'_2 and an A''_2 rotational symmetry species.

B. Hamiltonian Matrix

In agreement with the IAM-like approach, the tunneling-rotational Hamiltonian matrix is now set up using the refer-

TABLE 3
Transformation Properties of the Coordinates under the Operations[a] of the $D_{3h}(M)$ molecular symmetry group

Operations	Rotation[b]	Tunneling[c]
E	χ,θ,ϕ	$+\rho$
(123)	χ,θ,ϕ	$\rho + \frac{2\pi}{3}$
(23)	$\chi + \pi,\theta,\phi$	$-\rho$
E^*	$\pi - \chi,\pi - \theta,\pi + \phi$	$+\rho$

[a]The three operations selected allow us to generate the whole group.
[b]This column gives the effects of the operations on the Eulerian angles.
[c]This column gives the effects of the operations on the large amplitude coordinate ρ.

ence framework wavefunctions of Eq. [6]. We are thus led to consider matrix elements of the form

$$\langle \Psi_{JK'\alpha'm} | H | \Psi_{JK''\alpha''n} \rangle, \qquad [8]$$

where $\Psi_{JK'\alpha'm}$ and $\Psi_{JK''\alpha''m}$ are two reference framework wavefunctions. Because $1 \le m \le 3$ and $1 \le n \le 3$, the Hamiltonian matrix is of dimension $[3(2J + 1)] \times [3(2J + 1)]$. It can be decomposed into $(2J + 1)^2$ blocks of dimension 3×3, which are obtained by fixing the values of the rotational quantum numbers J, K', α', K'', and α'', but with $m, n = 1, 2$, or 3. The form of these blocks depends on the relative symmetry species of the rotational functions involved in the matrix elements of Eq. [8]. Using symmetry arguments, it can be shown that the matrix elements in these blocks are nonvanishing only in two cases. If both rotational symmetry species are identical, then the block is given by

$$\begin{bmatrix} H_0 & H_{1;2} & H_{1;2} \\ H_{1;2} & H_0 & H_{1;2} \\ H_{1;2} & H_{1;2} & H_0 \end{bmatrix}, \qquad [9]$$

where H_0 is a shorthand notation for the nontunneling matrix element $\langle \Psi_{JK'\alpha'1} | H | \Psi_{JK''\alpha''1} \rangle$; and $H_{1;2}$, for the tunneling matrix element $\langle \Psi_{JK'\alpha'1} | H | \Psi_{JK''\alpha''2} \rangle$. If the product of both rotational symmetry species is A_2', then the nondiagonal block has the following form:

$$\begin{bmatrix} 0 & H_{1;2} & -H_{1;2} \\ -H_{1;2} & 0 & H_{1;2} \\ H_{1;2} & -H_{1;2} & 0 \end{bmatrix}, \qquad [10]$$

where $H_{1;2}$ is defined as for the previous equation.

The calculation of the tunneling-rotation energy levels is greatly simplified if a block-diagonalization of the Hamiltonian matrix is carried out. This can be performed using symmetry-adapted linear combinations of reference framework wavefunctions, such as those given in Eq. [7], and allows us to split the Hamiltonian matrix into six blocks of different dimension. The matrix elements for the block corresponding to the symmetry species Γ will be written as

$$H(\Gamma)_{JK'\alpha';JK''\alpha''} = \langle \Psi_{JK'\alpha'\Gamma} | H | \Psi_{JK''\alpha''\Gamma} \rangle. \qquad [11]$$

Expressions for these matrix elements can be obtained from Eqs. [9] and [10]. When Γ is one of the four nondegenerate symmetry species, which implies that both rotational symmetry species are the same, then

$$H(\Gamma = A_1', A_2', A_1'', \text{or } A_2'')_{JK'\alpha';JK''\alpha''} = H_0 + 2H_{1;2}. \qquad [12]$$

When Γ is one of the two doubly degenerate symmetry species, the relative symmetries of the two rotational wave-

TABLE 4
Symmetry Species of the $|JK\alpha\rangle$ Functions of Eq. [5]

Label[a]	Γ (J even)	Γ (J odd)
E^+	A_1'	A_1''
E^-	A_1''	A_1'
O^+	A_2''	A_2'
O^-	A_2'	A_2''

[a]In this column asymmetric-top labels of the rotational functions are given. The letter E and O represent functions of even K and odd K, respectively. The superscripts + and − indicate that $\alpha = +1$ and $\alpha = -1$, respectively.

functions should be considered. When both rotational symmetry species are the same, then

$$H(\Gamma = E' \text{ or } E'')_{JK'\alpha';JK''\alpha''} = H_0 - H_{1;2}. \quad [13]$$

When the product of the two rotational symmetry species is A_2', then

$$H(\Gamma = E_a' \text{ or } E_a'')_{JK'\alpha';JK''\alpha''} = \pm\sqrt{3}H_{1;2}, \quad [14]$$

where the upper (lower) sign is for a $|JK'\alpha'\rangle$ rotational function of A_1' or A_1'' (A_2' or A_2'') symmetry. In Eqs. [12] and [13], the matrix elements of H_0 are those of a Watson-type Hamiltonian written with the *S*-reduced set of distortion constants and the I^r representation. The derivation of the matrix elements of $H_{1;2}$, which appears in Eqs. [12]–[14], will be carried out in the next subsection.

C. Hamiltonian Tunneling Matrix Elements

To write the Hamiltonian tunneling matrix element between the rovibrational wavefunction centered at configuration 1 and characterized by J and K', and the rovibrational wavefunction centered at configuration 2 and characterized by J and K'', we use Eq. (5) of Ref. (*11*)

$$H_{JK'1;JK''2} = h_{2v} \cdot D^{(J)}(\chi_2, \theta_2, \phi_2)_{K'',K'}, \quad [15]$$

where h_{2v} is a real factor arising from the vibrational integral along the tunneling path; and the three Eulerian-type angles χ_2, θ_2, and ϕ_2, in the IAM-like approach of Ref. (*10*), describe the rotational dependence of the tunneling splitting. Values for these angles are to be obtained, once the reference positions $\mathbf{a}_i(\rho)$ are known, solving Eqs. (7) and (8) of Ref. (*11*), which give the relation obeyed by the rotation $T^{-1}(\eta)$ such that $T^{-1}(\eta = +1) = S^{-1}(\chi_2, \theta_2, \phi_2)$. In the present case, due to the fact that the tunneling angular momentum is always parallel to the y axis of the molecule-fixed axis system, the only nonzero component of the $\boldsymbol{\omega}(\eta)$ vector will be $\omega_y(\eta)$, and $T^{-1}(\eta = +1)$ turns out to be a rotation about the y axis. For this reason two of the Eulerian-type angles of Eq. [15], namely, χ_2 and ϕ_2, will vanish.

Equation [15] can be rewritten making use of the reference framework wavefunctions of Eq. [6], the Hamiltonian tunneling matrix element takes then the form

$$\langle \Psi_{JK'\alpha'1}|H|\Psi_{JK''\alpha''2}\rangle = h_{2v}\langle JK'\alpha'|D(\theta_2)|JK''\alpha''\rangle, \quad [16]$$

where $D(\theta_2)$ is an operator whose matrix elements can be derived using the results of Ref. (*11*). We find

$$\langle JK'\alpha'|D(\theta_2)|JK''\alpha''\rangle = d^{(J)}(\theta_2)_{K'',K'} + \alpha' d^{(J)}(\theta_2)_{K'',-K'}, \quad [17]$$

if $\alpha'\alpha''(-1)^{K'+K''} = +1$, and

$$\langle JK'\alpha'|D(\theta_2)|JK''\alpha''\rangle = 0, \quad [18]$$

if $\alpha'\alpha''(-1)^{K'+K''} = -1$. Equation [17] is only valid if K' and $K'' > 0$; if either K' or K'' are zero, the expression on the right of the equation must be divided by $\sqrt{2}$; if both K' and K'' are zero, a division by 2 must be carried out. When expressed in terms of the symmetry species of the rotational functions, the requirement on the rotational quantum numbers for Eq. [17] means that the operator $D(\theta_2)$ has nonvanishing matrix elements between two rotational functions provided the product of their symmetry species is either A_1' or A_2', and this is consistent with Eqs. [9] and [10]. As can be gathered from Table 4, the latter condition implies, in terms of asymmetric-top labels, that if one of the rotational functions is E^+, E^-, O^+, or O^- then the other one must be O^-, O^+, E^-, or E^+, respectively. The expressions given in Eqs. [16], [17], and [18] account for the rotational dependence of the tunneling splitting; however, they do not include any rotation-like distortion contributions. Because these contributions may be important, Eq. [16] will be modified and various distortion operators will be introduced as in Ref. (*11*). The Hamiltonian tunneling matrix element thus takes the final expression

$$\langle \Psi_{JK'\alpha'1}|H|\Psi_{JK''\alpha''2}\rangle = \frac{1}{2}\langle JK'\alpha'|\{h_{2v} + h_{2j}\mathbf{J}^2 + h_{2k}J_z^2 + f_2(J_+^2 + J_-^2), D(\theta_2 + \theta_{2j}\mathbf{J}^2)\}|JK''\alpha''\rangle, \quad [19]$$

where h_{2j}, h_{2k}, f_2, and θ_{2j} are four constants; $\mathbf{J}$, J_x, J_y, and J_z are the total angular momentum and its components; $J_\pm = J_x \pm iJ_y$; $\{,\}$ is the anticommutator; and the operator D is defined in Eqs. [17] and [18].

4. ANALYSIS

The transitions measured in Refs. (*3*), (*4*), and (*7*) and those reported in the present work were included in a least-squares fit program in which they were given a weight equal to the square of the inverse of their experimental uncertainty. In this analysis the energy was calculated as shown in the previous section, diagonalizing the Hamiltonian submatrices given in Eqs. [12]–[14]. In addition to some of the parameters of the rotational Hamiltonian, the parameters of Eq. [19] were varied. Transitions for which the tunneling splitting or the *K*-type splitting could not be resolved were treated as follows: let f_1 and f_2 be the two frequencies of the unresolved doublet, the transition frequency was then calculated as $(f_1 + f_2)/2$ in the fitting procedure. A similar procedure also was applied to the unresolved quartets observed for

TABLE 5
Rotational and Tunneling Parameters[a] for $Ar \cdot H_3^+$ and $Ar \cdot D_3^+$

Constant		$Ar \cdot H_3^+$	$Ar \cdot D_3^+$
A		1 477 964.2(79000)	745 360.8(13000)
B		30 941.553 8(63)	16 517.556 5(83)
C		30 159.080 2(60)	16 099.304 4(69)
D_{JK}		35.749 8(54)	9.417 8(36)
D_J		0.541 22(10)	0.155 289(15)
d_1	$\times 10^3$	−11.302(13)	−3.304(13)
d_2	$\times 10^3$	−1.538(39)	−0.361 8(84)
H_{KKJ}	$\times 10^3$	−211.0(16)	−33.3(13)
H_{KJJ}	$\times 10^6$	−644.(74)	−77.3(78)
H_J	$\times 10^6$	−30.38(31)	−4.124(13)
h_1	$\times 10^9$		−64.(16)
h_2	$\times 10^9$		14.1(96)
L_{KKJ}	$\times 10^3$		−1.35(11)
L_{KJ}	$\times 10^6$		−58.1(85)
h_{2v}		−1 136.25(17000)	−31.15(2900)
h_{2kj}	$\times 10^3$	−493.39(220)	−2.04(51)
θ_2		3.816 3(2900)	2.107(1000)
θ_{2j}	$\times 10^3$	−0.412 30(6800)	

[a] All parameters are given in MHz, except θ_2 and θ_{2j}, which are in degrees. Numbers in parentheses are one standard deviation in the same units as the last digit. In the body of the table, a blank entry means that the constant was fixed to zero.

$Ar \cdot D_3^+$. Forty transitions were fitted with a unit-less standard deviation of 0.65, in the case of $Ar \cdot H_3^+$, and 73 transitions with a less satisfactory standard deviation of 1.77, in the case of $Ar \cdot D_3^+$. Table 1 lists the assignment, the observed frequency, and observed minus calculated difference for each transition of $Ar \cdot H_3^+$. In this table, no rovibrational levels of species A_1' or A_1'' in $D_{3h}(M)$ appear as they are missing in the $Ar \cdot H_3^+$ spectrum because of nuclear spin statistics. Table 2 lists the same quantities as Table 1, but for $Ar \cdot D_3^+$. The parameters determined in both analyses, along with their uncertainty, appear in Table 5.

5. STRUCTURAL CALCULATION

In the present section we make use of some of the parameters determined in the line frequency analysis in order to obtain quantitative information on the geometry of the molecule at the intermediate configuration for the large amplitude motion. For this purpose, the angle θ_2, describing the rotational dependence of the tunneling splitting, will be considered. Starting from a reasonable guess at the reference positions $\mathbf{a}_i(\rho)$; this angle will be calculated theoretically (see Section 3.C) and compared with the value obtained in the analysis. The reference positions then will be adjusted slightly in order to match theoretical and observed values for this angle. Unfortunately, this procedure only can be applied to the normal species of the complex because it is only for that species that a reliable value for the angle θ_2 could be obtained as all tunneling splittings could be experimentally resolved.

The calculation will be carried out using two models, which will be referred to as models I and II. For both models, the nonzero components of the reference positions will be expressed as follows:

$$a_i'(\rho)_x = -r_i(\rho)\sin\left[\rho + (i-1)\frac{2\pi}{3}\right],$$
$$a_i'(\rho)_z = -r_i(\rho)\cos\left[\rho + (i-1)\frac{2\pi}{3}\right], \quad [20]$$

where $i = 1$, 2, or 3 for the three hydrogen atoms, and

$$a_0'(\rho)_z = -R(\rho), \quad [21]$$

for the argon atom. In these three equations, the prime sign indicates that the reference positions components are given in an $x'y'z'$-axis system, which was chosen for convenience, but which differs from the molecule-fixed axis system of Section 3.A by a ρ-dependent translation.

A. Model I

This first model is very crude and is based on the one used by Escribano and Bunker (*6*). As these authors, we assume that the H_3^+ triangle is rigid and unchanged on complexation; the H–H distance being equal to its zero point value: 0.8763 Å. However, the distance between the argon atom and the center of mass of the H_3^+ ion will be made ρ dependent and will be such that it is equal to the value obtained by Bunker and Escribano at the equilibrium configuration: 2.38522 Å. This leads to

$$r_i(\rho) = 0.8763\ \text{Å}/\sqrt{3}, \qquad i = 1, 2, \text{ or } 3,$$
$$R(\rho) = 2.38522\ \text{Å} + Q_3(1 - \cos 3\rho). \quad [22]$$

Escribano and Bunker's model (*6*) correspond to $Q_3 = 0$ and this yields a calculated value for θ_2 of 5.54°. The expected value 3.81°, as can be gathered from Table 5, is much smaller than that. An adjustment of Q_3 was, therefore, performed and led to $Q_3 = 0.59$ Å. This means that at the intermediate configuration the argon atom is more than 1 Å farther from the H_3^+ ion than at the equilibrium configuration.

B. Model II

This second model is more refined because it allows the H_3^+ ion to be distorted from its equilateral triangle shape. In agreement with Ref. (*4*), we assumed the following formulas:

$$r_i(\rho) = \sum_{n=0}^{3} P_n \cos n\left[\rho + (i-1)\frac{2\pi}{3}\right],$$

$$i = 1, 2, \text{ or } 3, \qquad [23]$$

$$R(\rho) = Q_0 + Q_3 \cos 3\rho,$$

which are equivalent to those given in Section III.B.1 of Ref. (*4*). Values for the various parameters appearing in these equations are to be taken from Table XV of this reference. In this case, we obtain a calculated value for θ_2 of 5.07°, again too large, but not as much as with model I. Parameters Q_0 and Q_3 were therefore both adjusted; the sum $Q_0 + Q_3$ being held fixed to 2.412 Å so that the equilibrium configuration described by Eqs. [20], [21], and [23] be the same as the one of Ref. (*4*). This yielded $Q_0 = +3.059$ Å and $Q_3 = -0.647$ Å. The parameter Q_0 has been increased of 0.51 Å while Q_3 has been decreased by the same amount. At the equilibrium configuration, with these values, the argon atom is 1 Å farther from the H_3 ion than predicted in Ref. (*4*).

The results obtained with models I and II are consistent and suggest that in the planar intermediate configuration for the large amplitude motion the argon atom is much farther away from the H_3^+ ion than assumed previously (*4–6*). This result, however, should be taken with care because it was obtained from the analysis of a limited number of transitions. This disagreement also may be due to the inadequateness of the present theoretical approach in which only one tunneling path was considered. Contributions from tunneling paths characterized by a nonplanar intermediate configuration, such as the one identified by number 3 in Fig. 1 of Ref. (*5*), may have prevented us from obtaining a reliable value for the angle θ_2.

6. CONCLUSION

In this paper an investigation of the sub-millimeter-wave spectra of $Ar \cdot H_3^+$ and $Ar \cdot D_3^+$ up to 680 GHz was presented. Thanks to the enhanced sensitivity of the spectrometer, a significant number of submillimeter rotational transitions could be observed and the first $K_a = 2$ and $K_a = 3$ lines for respectively $Ar \cdot H_3^+$ and $Ar \cdot D_3^+$ could be recorded. These transitions together with already available data (*3, 4, 7*) were analyzed by means of a theoretical approach, which accounts for the large amplitude motion displayed by the two species. Assuming that this motion is a planar 120° rotation of the H_3^+ or the D_3^+ moieties allows us to reproduce satisfactorily the transition frequencies and to retrieve values for the tunneling splitting in both species (see Table 5). Such a determination, impossible solely from the line frequencies, is accomplished here because the theoretical model accounts for the tunneling-splitting-rotational dependence. The theoretical model also allows us to extract information concerning the geometry of the intermediate configuration for the large amplitude motion. This latter result, at least for the normal species, seems to disagree with the structures obtained previously (*4, 6*).

ACKNOWLEDGMENT

The Laboratoire de Spectroscopie Hertzienne is a ''Unité de Recherche Associée au CNRS'' and the Laboratoire de Photophysique Moléculaire is a ''Laboratoire Propre du CNRS.'' The Centre d'études et de Recherches Lasers et Applications is supported by the Ministère Chargé de la Recherche, the Région Nord-Pas de Calais and by the Fonds Européeens de Développement Economique des Régions. The acquisition of new BWOs was funded in part by an INSU grant from the CNRS. M. Yu. T. thanks the European Union (PECO Contract CIPDCT 94-0614), A. F. K. thanks the Nord-Pas de Calais Region, and S. C. thanks the CNRS for supporting their stay in Lille. Russian side of studies was supported in part by Russian Fund for Basic Research (RFBR) Grant N 97-02-16593.

REFERENCES

1. Y. Ohshima, Y. Sumiyoshi, and Y. Endo, *J. Chem. Phys.* **106,** 2977–2979 (1997).
2. T. Ruchti, T. Speck, E. J. Bieske, H. Linnartz, and J. P. Maier, ''Fifteenth Colloquium on High Resolution Molecular Spectroscopy, Glasgow, September 7–11,'' Paper F26, 1997.
3. M. Bogey, H. Bolvin, C. Demuynck, and J.-L. Destombes, *Phys. Rev. Lett.* **58,** 988–991 (1987).
4. M. Bogey, H. Bolvin, C. Demuynck, J.-L. Destombes, and B. P. van Eijck, *J. Chem. Phys.* **88,** 4120–4126 (1988).
5. E. D. Simandiras, J. F. Gaw, and N. C. Handy, *Chem. Phys. Lett.* **141,** 166–174 (1987).
6. R. Escribano and P. R. Bunker, *Chem. Phys. Lett.* **143,** 439–444 (1988).
7. Y. Ohshima and Y. Endo, *Chem. Phys. Lett.* **256,** 635–640 (1996).
8. G. Winnewisser, A. F. Krupnov, M. Yu. Tretyakov, M. Liedtke, F. Lewen, A. H. Saleck, R. Schieder, A. P. Shkaev, and S. V. Volokhov, *J. Mol. Spectrosc.* **165,** 294–300 (1994).
9. M. Bogey, S. Civiš, B. Delcroix, C. Demuynck, A. F. Krupnov, J. Quiguer, M. Yu. Tretyakov, and A. Walters, *J. Mol. Spectrosc.* **182,** 85–97 (1997).
10. J. T. Hougen, *J. Mol. Spectrosc.* **114,** 395–426 (1985).
11. L. H. Coudert and J. T. Hougen, *J. Mol. Spectrosc.* **130,** 86–119 (1988).
12. L. H. Coudert, *J. Mol. Spectrosc.* **132,** 13–34 (1988).
13. D. Christen, L. H. Coudert, R. D. Suenram, and F. J. Lovas, *J. Mol. Spectrosc.* **172,** 57–77 (1995).
14. M. Cordonnier and L. H. Coudert, *J. Mol. Spectrosc.* **178,** 59–65 (1996).
15. M. Bogey, H. Bolvin, M. Cordonnier, C. Demuynck, J.-L. Destombes, and A. G. Császár, *J. Chem. Phys.* **100,** 8614–8624 (1994).
16. J.-L. Destombes, M. Bogey, M. Cordonnier, C. Demuynck, and A. Walters, *in* ''Conference Proceedings of the American Institute of Physics, No. 312,'' (I. Nenner, Ed.), p. 268, 1994.
17. P. R. Bunker, ''Molecular Symmetry and Spectroscopy.'' Academic Press, New York, 1979.